SCIENTIFIC REPORTS

OPEN

Effect of ionic radii on the Curie temperature in $Ba_{1-x-y}Sr_xCa_yTiO_3$ compounds

Received: 05 March 2016
Accepted: 31 May 2016
Published: 21 June 2016

A. Berenov, F. Le Goupil & N. Alford

A series of $Ba_{1-x-y}Sr_xCa_yTiO_3$ compounds were prepared with varying average ionic radii and cation disorder on A-site. All samples showed typical ferroelectric behavior. A simple empirical equation correlated Curie temperature, T_C, with the values of ionic radii of A-site cations. This correlation was related to the distortion of TiO_6 octahedra observed during neutron diffraction studies. The equation was used for the selection of compounds with predetermined values of T_C. The effects of A-site ionic radii on the temperatures of phase transitions in $Ba_{1-x-y}Sr_xCa_yTiO_3$ were discussed.

Perovskites with the general formula: $Ba_{1-x-y}Sr_xCa_yTiO_3$ (BSCT) show enhancement of several properties (e.g dielectric, piezoelectric[1], electrocaloric[2] response) in the vicinity of Curie temperature, T_C, where a cubic to tetragonal phase transition occurs and could be strong contenders for Pb-free ferroelectric materials[3]. As a result, the ability to optimize chemical composition of BSCT compounds in order to shift T_C to the desired operating temperature range is important from a practical point of view. Several decades of research have established some of the key parameters that influence the T_C in perovskites: chemical composition of A- and B-sites in ABO_3 perovskites[4], A to B nonstoichiometry ratio[5], lattice parameters[6], tolerance factor[7], average mass of A-site ions[8], $^{18}O/^{16}O$ isotope ratio[9], grain size[10], annealing temperature[11], hydrostatic pressure[12], strain in thin film[13]. Nevertheless there is still a lack of simple guidelines for the selection of the materials compositions with predetermined value of T_C.

The average ionic radius, $<r_{A-site}>$, of A-site ions has a strong effect on the T_C especially in $Ba_{1-x}Sr_xTiO_3$ compounds where T_C decreases linearly with Sr doping. This decrease is usually explained by the substitution of Ba ions by smaller Sr ions resulting in the observed linear decrease of the T_C with lattice parameter in $Ba_{1-x}Sr_xTiO_3$ (a or $\sqrt[3]{a^2c}$) for cubic or tetragonal phases, respectively)[6]. Similarly, the decrease T_C with applied hydrostatic pressure[12] was explained by the pressure induced decrease of the unit cell volume[14].

Another parameter affecting T_C is the A-site cation disorder which can be quantified by variance, σ^2, as follows[15]

$$\sigma^2 = \sum y_i r_i^2 - <r_{A-site}>^2 \quad (1)$$

where r_i and y_i–ionic radii and occupancy of A-site of element i, respectively. The linear increase of the T_C with σ^2 in BSCT has been observed when the average ionic radius was kept constant[16]. In other perovskite or perovskite related structures, the increase of σ^2 was shown to decrease the metal-insulator transition temperature in manganites[15] and decrease critical current in YBCO-type superconductors[17]. In this work we evaluated the effects of average ionic radius (ionic radii in 12 fold coordination were used[18]) and ionic radii variance of A-site ions in the perovskite lattice on the phase transitions in BSCT compounds.

A series of compounds (see Table 1) were prepared by a conventional solid-state reaction synthesis with starting chemicals $BaCO_3$ (Alfa Aesar, 99.95%), $CaCO_3$ (Alfa Aesar, 99.95%), $SrCO_3$ (Alfa Aesar, 99.99%) and TiO_2 (PI-KEM Ltd., 99.9%) calcined at 1300 °C for 10 hrs. Three series of compounds were prepared: series A where $<r_{A-site}>$ was fixed at 1.551 Å and σ^2 was varied from 0.0066 to 0.0125 Å^2, series B where both $<r_{A-site}>$ and σ^2 were varied, series C where both $<r_{A-site}>$ and σ^2 were varied in order to maintain constant T_C as described below. Chemical composition was confirmed by ICP-OES analysis (DV 200 OES, Perkin Elmer). XRD (X'PERT MPD, PANalytical) showed that all specimens were single phase tetragonal perovskites (4 mm s.g.) at room temperature except for $Ba_{0.78}Ca_{0.22}TiO_3$ where a weak peak belonging to $CaTiO_3$ was observed (see Supplementary Fig. S1). This composition is close to the temperature dependent Ca solubility limit of 16% at 1300 °C[19], 25% at 1430 °C[20]

Department of Materials, Imperial College London, London, SW7 2AZ, UK. Correspondence and requests for materials should be addressed to A.B. (email: a.berenov@imperial.ac.uk)

Composition	$<r_{A-site}>$ (Å)	δ^2 (Å^2)	a (Å)	c (Å)	c/a
Series A					
$Ba_{0.65}Sr_{0.35}TiO_3$	1.5505	0.0066	3.9657(1)	3.9739(1)	1.0021
$Ba_{0.69}Sr_{0.24}Ca_{0.07}TiO_3$	1.5505	0.0085	3.9655(4)	3.9831(8)	1.0044
$Ba_{0.74}Sr_{0.12}Ca_{0.15}TiO_3$	1.5506	0.0105	3.9633(6)	3.9938(8)	1.0077
$Ba_{0.78}Ca_{0.22}TiO_3$	1.5506	0.0125	3.9631(7)	4.0066(9)	1.0110
Series B					
$Ba_{0.8}Sr_{0.2}TiO_3$	1.5760	0.0046	3.9804(1)	4.0045(4)	1.0061
$Ba_{0.6}Sr_{0.2}Ca_{0.2}TiO_3$	1.5220	0.0126	3.9500(1)	3.9640(5)	1.0036
$Ba_{0.9}Ca_{0.1}TiO_3$	1.5830	0.0066	3.9784(1)	4.0236(1)	1.0114
$Ba_{0.85}Sr_{0.1}Ca_{0.05}TiO_3$	1.5795	0.0056	3.9793(2)	4.0149(2)	1.0089
$Ba_{0.78}Sr_{0.1}Ca_{0.12}TiO_3$	1.5606	0.0092	3.9696(2)	4.0043(2)	1.0088
$Ba_{0.75}Sr_{0.1}Ca_{0.15}TiO_3$	1.5525	0.0105	3.9609(2)	3.9956(3)	1.0088
$Ba_{0.7}Sr_{0.1}Ca_{0.2}TiO_3$	1.5390	0.0124	3.9576(2)	3.9884(2)	1.0078
Series C					
$Ba_{0.68}Sr_{0.32}TiO_3$	1.5559	0.0063	3.9688(1)	3.9795(3)	1.0027
$Ba_{0.62}Sr_{0.28}Ca_{0.1}TiO_3$	1.5359	0.0098	3.9580(1)	3.9683(4)	1.0026

Table 1. Crystallographic parameters of studied samples.

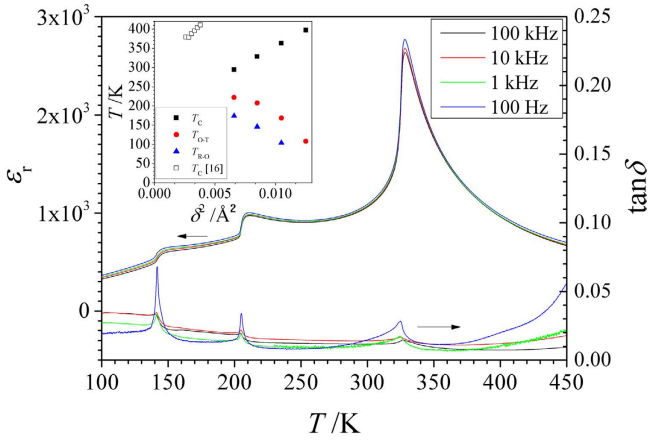

Figure 1. Temperature dependence of permittivity and loss tangent of $Ba_{0.69}Sr_{0.24}Ca_{0.07}TiO_3$ at 0.1, 1, 10 and 100 kHz. Measurements were performed during 1 K min^{-1} heating. Inset shows temperatures of phase transitions in BSCT compounds (series A) as a function of σ^2.

and 1549 °C[21]. A good agreement between the values of the lattice parameters of $Ba_{1-x}Sr_xTiO_3$ with those reported in the literature[22] was observed. For the series A the increase of variance resulted in a slight decrease of the a lattice parameter and increase of the c lattice parameter whereas the c/a ratio showed an increase. Dense pellets (>92% dense) were prepared by sintering at 1450 °C. The average grain size was 30–65 μm as observed by SEM (JSM 6400, JEOL) and shown in Supplementary Fig. S2. DSC measurements (DSC200 F3, Netzch) during 5 K/min heating showed well defined peaks at T_{R-O}, T_{O-T} and T_C which correspond to consecutive phase transitions during heating from rhombohedral (3 m) to orthorhombic (mm2) to tetragonal (4 mm) and, finally, to cubic (m3 m) structures, respectively (see Supplementary Fig. S3 and Supplementary Table S4).

The dielectric properties were evaluated by HP 4263B LCR with 0.3 V/mm ac signal at 0.1–100 kHz. The thermal hysteresis observed between heating and cooling runs was less than 3 K. Dielectric permittivity, ε_r, peaked at T_C and showed humps at T_{R-O} and T_{O-T} (Fig. 1). No frequency dependence of ε_r was observed. The tanδ showed clear peaks positioned slightly below (by less than 10 K) the temperatures of the corresponding phase transitions. The estimated error in the determination of temperatures of phase transitions is 1.5 K and a good agreement was observed between the values of T_C, T_{R-O} and T_{O-T} determined from DSC and LCR measurements. Both T_{R-O} and T_{O-T} decreased with Ca doping and no T_{R-O} and T_{O-T} were observed in the samples with more than 20 and 15% of Ca doping, respectively, in agreement with the literature[23,24]. T_C increases linearly with the tetragonal distortions in the lattice (expressed as c/a ratio) regardless of the chemical composition of samples (Supplementary Fig. S5). The ε_r data located 10–20 K above T_C were fitted to the Curie-Weiss law (Table 2). The value of T_0 determined from the fitting, was smaller than T_C suggesting a first order phase transition in all studied samples.

It has been shown that the increase of cation disorder results in the formation of relaxor type behavior[25]. As a result a modified Curie-Weiss law[26] was used to fit the data

Composition	$T_{R\text{-}O}$ (K)	$T_{O\text{-}T}$ (K)	T_C (K)	ε_{rm}	T_0 (K)	γ
Series A						
$Ba_{0.65}Sr_{0.35}TiO_3$	174	222	294	2566	271	1.09
$Ba_{0.69}Sr_{0.24}Ca_{0.07}TiO_3$	146	208	328	2635	289	1.03
$Ba_{0.74}Sr_{0.12}Ca_{0.15}TiO_3$	104	167	363	6132	351	1.12
$Ba_{0.78}Ca_{0.22}TiO_3$	NA	NA	397	4049	373	1.19
Series B						
$Ba_{0.8}Sr_{0.2}TiO_3$	187	253	343	4483	322	1.11
$Ba_{0.6}Sr_{0.2}Ca_{0.2}TiO_3$	NA	NA	324	2692	301	1.18
$Ba_{0.9}Ca_{0.1}TiO_3$	148	231	411	2994	385	1.27
$Ba_{0.85}Sr_{0.1}Ca_{0.05}TiO_3$	172	250	378	4251	365	1.15
$Ba_{0.78}Sr_{0.1}Ca_{0.12}TiO_3$	134	206	375	3697	360	1.21
$Ba_{0.75}Sr_{0.1}Ca_{0.15}TiO_3$	NA	170	373	3161	357	1.25
$Ba_{0.7}Sr_{0.1}Ca_{0.2}TiO_3$	NA	94	363	3826	353	1.24
Series C						
$Ba_{0.68}Sr_{0.32}TiO_3$	176	229	304	3737	269	1.08
$Ba_{0.62}Sr_{0.28}Ca_{0.1}TiO_3$	124	184	311	9564	309	1.18

Table 2. The results of dielectric measurements of studied compounds.

$$\frac{1}{\varepsilon_r} - \frac{1}{\varepsilon_{rm}} = \frac{(T - T_m)^\gamma}{C} \tag{2}$$

where ε_{rm} is the permittivity at T_C, γ is exponent which is expected to be 1 for classical ferroelectrics and 2 for relaxors. Relatively low values of γ measured in this work (1.03–1.27), the lack of frequency dependence of ε_r and the closeness of the peaks on ε_r and δ temperature curves, suggested that all compounds investigated showed typical ferroelectric behavior. The linear increase of the T_C with the σ^2 was observed (inset Fig. 1). The observed $\frac{\partial T_C}{\partial \delta^2}$ slope was slightly larger (17252 K Å^{-1}) than previously reported (14500 K Å^{-1}) for BSCT compounds with $<r_{A-site}> = 1.594$ Å[16]. $T_{T\text{-}O}$ and $T_{R\text{-}O}$ showed a monotonic decrease with σ^2.

Recently a combined effect of the average ionic radii and cation variance on the phase transition temperature in perovskite (alkaline earth doped rare earth manganites) and perovskite related (cuprate superconductors) compounds was proposed[27]. For example, a linear decrease of the metal-insulator transition temperature with the increase of the $\sigma^2 + (<r_{A-site}> - r^0_{A-site})^2$ function was observed in a large number of manganites[28]. r^0_{A-site} is the ionic radius of the "ideal" non-distorted cubic perovskite which can be calculated from geometrical considerations as $r^0_{A-site} = \sqrt{r_{B-site} + r_O} - r_O$ where r_{B-site} and r_O are ionic radii of B and O ions in ABO_3 perovskite, respectively. An empirical hard sphere ionic model has been proposed[28] where the increase in σ^2 and $(<r_{A-site}> - r^0_{A-site})^2$ determined BO_6 octahedra tilting in perovskites with the tolerance factor, t, less than 1 and introduced strain like energy term affecting the temperature of phase transition. Similar hard sphere ionic model was applied to the perovskites studied in this work with the $t > 1$. In this case the lattice distortions caused by ion size mismatch relieved not by BO_6 octahedra tilting but by shifting of oxygen ions leading to the distortion of BO_6 octahedra[29]. In the model the ferroelectricity was assumed to be caused by the shift of Ti ions in the direction of equatorial oxygen in TiO_6 octahedra however the results of local-structure refinements in Sr doped $BaTiO_3$ suggested 4 site distribution of Ti ions in tetragonal and 8 site distribution in cubic phases with the site splitting of ≈0.2 Å[29,30]. In the ideal non-distorted cubic perovskite ($t = 1$) Ti and O ions were closely packed and no shift of Ti ions from the centrosymmetric positions were possible (Fig. 2(a)). An increase of $<r_{A-site}>$ by the introduction of larger A-site ions ($\sigma^2 = 0$ Fig. 2(b)) or an increase of σ^2 by the introduction of cation disorder ($<r_{A-site}> = r^0_{A-site}$ Fig. 2(c)) was likely to enlarge TiO_6 octahedra and allowed Ti ions to shift from the centrosymemtric position at $T < T_C$ by the distance d. From the geometrical considerations:

$$d^2 = \frac{1}{2}(<r_{A-site}> - r^0_{A-site})^2 \tag{3}$$

and (assuming $\frac{1}{2}(2r^0_{A-site} + 2r_O)^2 \gg \sigma^2$)

$$d^2 \cong \frac{1}{4}\sigma^2 \tag{4}$$

for the former (Fig. 2(b)) and later (Fig. 2(c)) cases, respectively. It has been shown both empirically[31] and theoretically[32,33] that T_C depends on the atomic displacement of B-site cations, d, as $T_C \sim d^2$.

As a result an increase of the T_C with both $(<r_{A-site}> - r^0_{A-site})^2$ and σ^2 was expected. However a poor correlation of values of T_C with $\sigma^2 + (<r_{A-site}> - r^0_{A-site})^2$ function was observed for the samples studied in this work (Supplementary Fig. S6) presumably due to the assumptions used in the suggested simple model (spherical

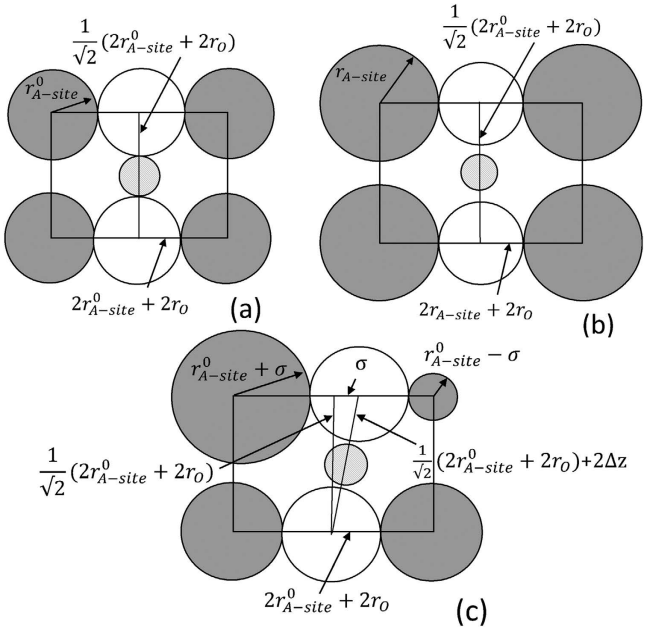

Figure 2. Schematic representation of (110) planes in the ideal cubic perovskite with $<r_{A-site}> = r^0_{A-site}$ and $\sigma^2 = 0$ (**a**), in the cubic perovskite with $<r_{A-site}> > r^0_{A-site}$ and $\sigma^2 = 0$ (**b**) and in the cubic perovskite with $<r_{A-site}> = r^0_{A-site}$ and $\sigma^2 > 0$ (**c**). Grey, white, and patterned circles represent A-site ions, O and Ti ions, respectively.

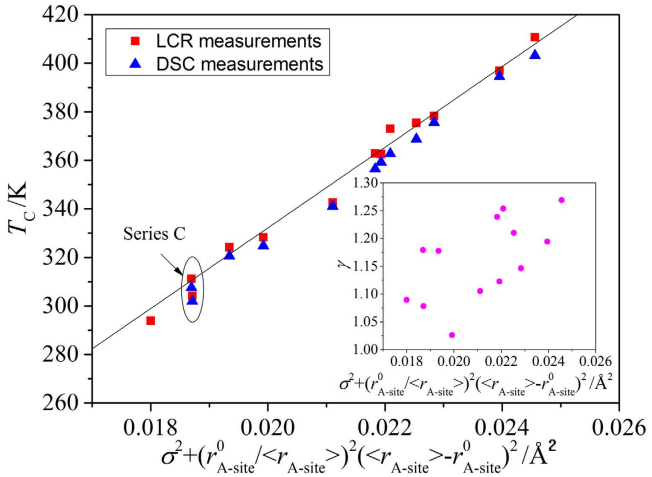

Figure 3. T_C as a function of $\sigma^2 + \left(\frac{r^0_{A-site}}{<r_{A-site}>}\right)^2 (<r_{A-site}> - r^0_{A-site})^2$. Solid line is a fit to equation 3. Inset shows γ as function of $\sigma^2 + \left(\frac{r^0_{A-site}}{<r_{A-site}>}\right)^2 (<r_{A-site}> - r^0_{A-site})^2$.

non polarizing ions, cubic perovskite structure in the ferroelectric phase, neglect of off centered Ca ions, etc.) and a modified empirical function $\sigma^2 + \left(\frac{r^0_{A-site}}{<r_{A-site}>}\right)^2 (<r_{A-site}> - r^0_{A-site})^2$ was suggested.

The T_C of all studied samples showed a linear correlation with the modified function regardless of the cation composition on A-site (Fig. 3) as follows:

$$T_C[K] = 17252 \times \left[\sigma^2 + \left(\frac{r^0_{A-site}}{<r_{A-site}>}\right)^2 (<r_{A-site}> - r^0_{A-site})^2\right] - 16.9 \quad (5)$$

Although the proposed simple model appeared to qualitatively explain the empirical relationship of σ^2 and $<r_{A-site}>$ with T_C, a detailed model is required to relate ionic radii of individual ions with the following factors influencing ferroelectricity in titanate perovskites: magnitude of Ti off centering in TiO_6 octahedra, the direction

Parameter	Series A			Series B		Series C
	$Ba_{0.69}Sr_{0.24}Ca_{0.07}TiO_3$	$Ba_{0.74}Sr_{0.12}Ca_{0.15}TiO_3$	$Ba_{0.78}Ca_{0.22}TiO_3$	$Ba_{0.8}Sr_{0.2}TiO_3$	$Ba_{0.6}Sr_{0.2}Ca_{0.2}TiO_3$	$Ba_{0.68}Sr_{0.32}TiO_3$
a (Å)	3.96435(3)	3.96279(3)	3.96231(7)	3.97818(4)	3.94981(4)	3.96849(3)
c (Å)	3.98716(5)	3.99661(4)	4.00921(9)	4.00558(6)	3.97230(7)	3.98159(4)
z (A-site)	0.514(2)	0.512(14)	0.509(2)	0.512(2)	0.511(3)	0.519(2)
Uiso(A-site) ($Å^2$)	0.0056(2)	0.0097(2)	0.0073(3)	0.0079(2)	0.0106(2)	0.0070(2)
Uiso (Ti) ($Å^2$)	0.0033(4)	0.0071(3)	0.0050(4)	0.0071(4)	0.0064(5)	0.0042(4)
z (O1)	0.530(2)	0.5332(1)	0.536(1)	0.527(1)	0.529(2)	0.529(1)
Uiso (O1) ($Å^2$)	0.0079(6)	0.0115(4)	0.0100(5)	0.0098(5)	0.0140(7)	0.0093(5)
z (O2)	0.029(1)	0.030(1)	0.031(1)	0.029(1)	0.029(2)	0.031(1)
Uiso (O2) ($Å^2$)	0.0058(3)	0.0101(2)	0.0080(3)	0.0087(3)	0.0095(3)	0.0071(3)
wRp	4.11	4.34	5.90	4.17	4.11	4.15
Ti-O1 (Å)	1.876(6)	1.866(4)	1.861(5)	1.873(5)	1.870(7)	1.875(5)
Ti-O1 (Å)	2.111(6)	2.131(4)	2.148(5)	2.133(5)	2.102(7)	2.107(5)
Ti-O2 (Å)	1.9856(3)	1.9851(2)	1.9850(3)	1.9924(3)	1.9782(4)	1.9881(3)
Ti-O-Ti (°)	173.2(3)	173.0(2)	172.9(3)	173.4(3)	173.4(4)	172.9(2)
A-O1 (Å)	2.8039(1)	2.8034(1)	2.8039(2)	2.8143(1)	2.7938(1)	2.8604(7)
A-O2 (Å)	2.767(3)	2.762(3)	2.756(3)	2.774(3)	2.753(4)	2.778(3)
A-O2 (Å)	2.857(4)	2.862(3)	2.882(4)	2.872(3)	2.850(4)	2.844(3)

Table 3. Refined parameters obtained from Rietveld refinements on neutron data.

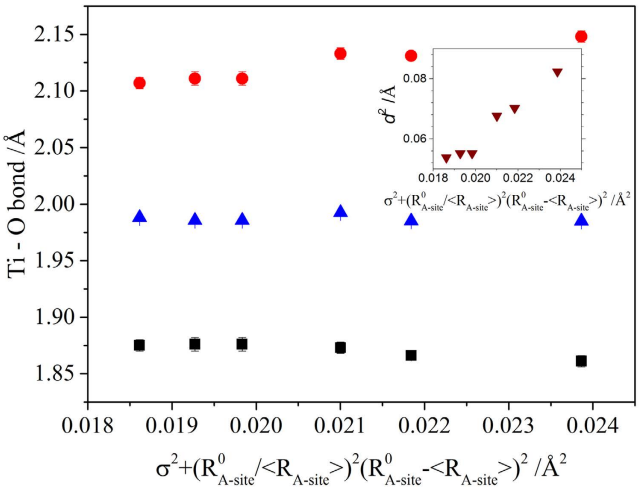

Figure 4. Ti-O bond lengths as a function of $\sigma^2 + \left(\frac{r^0_{A-site}}{<r_{A-site}>}\right)^2 (<r_{A-site}> - r^0_{A-site})^2$. Inset shows d^2 as function of $\boldsymbol{\sigma^2 + \left(\frac{r^0_{A-site}}{<r_{A-site}>}\right)^2 (<r_{A-site}> - r^0_{A-site})^2}$.

of the Ti off centering and contributions from A-site ions displacements. Recent studies of local structure provided vital information on the influence of Ca and Sr substitution in $BaTiO_3$ on the above mentioned parameters[29,30,34]. The magnitude of Ti off centering was found to decrease monotonically with Sr doping in $BaTiO_3$ as TiO_6 octahedra became more regular and reduced in volume[29,30,35]. This effect is usually associated with the observed decrease of T_C upon Sr doping. The effect of Ca doping on TiO_6 octahedra remains controversial. It was shown that Ca doping decreased the average volume of TiO_6 octahedra whereas the degree of distortions in TiO_6 network increased[35]. The volume of some TiO_6 octahedra was found to be close to the one of $BaTiO_3$ even when 30% Ca was introduced on A-site. On the other hand the increase of the volume of TiO_6 octahedra with the increasing number of neighboring Ca ions and concurrent increase of the Ti displacement was reported[30]. The direction of Ti ions displacement was found to be aligned at ≈33° with respect to the c axis in $BaTiO_3$[29]. Sr doping increased this angle of alignment to 39° in $Ba_{0.8}Sr_{0.2}TiO_3$ and 54° (Ti displacement along (111) direction) in $Ba_{0.5}Sr_{0.5}TiO_3$. As a result the c-axis component of polarization diminished lowering the value of T_C. Ca doping appeared to induce an opposite effect as the direction of Ti ions displacement was closely aligned with c axis in $Ba_{0.7}Ca_{0.3}TiO_3$[30]. No Sr off-centering was observed in $Ba_{1-x}Sr_xTiO_3$ materials resulting in an isotropic relaxation of oxygen ions around the A-site thus providing no additional contribution to specimen polarisation[29,30]. Ca off-centering was experimentally observed by EXAFS in $CaTiO_3$[34] and $Ba_{1-x}Ca_xTiO3$ ($0 < x < 0.5$)[30], by XANES in

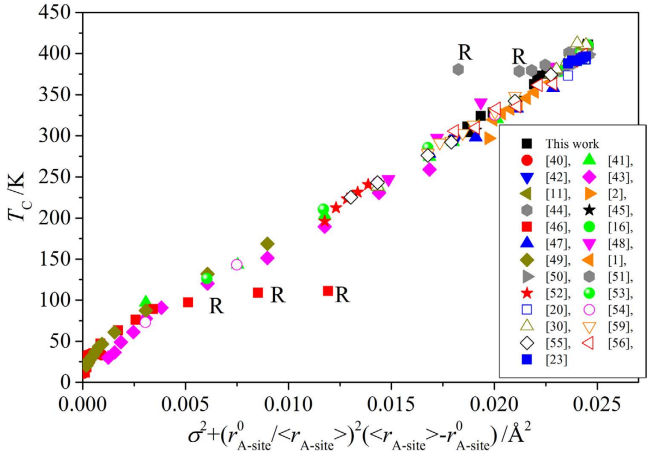

Figure 5. T_C as a function of $\sigma^2 + \left(\frac{r^0_{A-site}}{<r_{A-site}>}\right)^2 (<r_{A-site}> - r^0_{A-site})^2$ for samples studied in this work and reported in the literature. R denotes samples with relaxor type behavior.

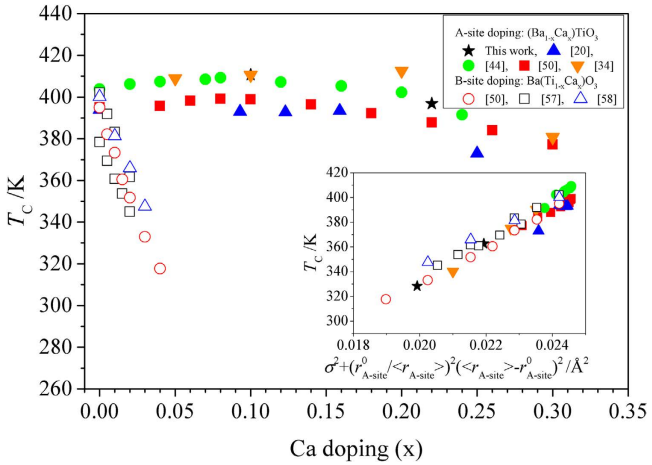

Figure 6. T_C as a function of Ca doping and $\sigma^2 + \left(\frac{r^0_{A-site}}{<r_{A-site}>}\right)^2 (<r_{A-site}> - r^0_{A-site})^2$ (inset).

$Ba_{1-x}Ca_xTiO_3$ (x = 0.02, 0.05)[36] compounds and theoretically predicted in $Ba_{0.875}Ca_{0.125}TiO_3$[24] and $Ba_{1-x}Ca_xTiO_3$[35]. If Ca off-center displacements occur in the same direction as TiO_6 distortions this additional contribution to polarization results in the increased values of T_C. The direction of Ca off-centering were reported along [111][30], [001][35,36] or [113][24] directions. Furthermore Ca displacements were shown to facilitate Ti displacements inside TiO_6 octahedra further enhancing ferroelectic behaviour[30]. It is possible to speculate that the increase of A-site cation disorder (expressed as σ^2) could facilitate the shift of smaller A-site cations from the centrosymmetric positions in order to relieve an associated bond strain. A model was proposed that assumed two competitive effects active during Ca doping in $Ba_{1-x}Ca_xTiO_3$: the shrinkage of TiO_6 octahedra resulting in smaller Ti displacements (and possibly away from the c-axis direction) and the increase of the number of off-centered Ca ions. This mode described experimentally observed T_C dependence reasonably well[35]. Similar A-site driven ferroelectricity was found in perovskites with the $t < 1$ where the introduction of smaller ions (e.g. Li in $K_{0.5}Li_{0.5}NbO_3$[37] and Lu in (La,Lu)$MnNiO_6$[38] stabilized off-centering of A-site ion (thus inducing ferroelectric state) over tilting of BO_6 octahedra[3].

The observed increase of T_C with σ^2 and decrease of T_C with $<r_{A-site}>$ are in agreement with previous results[16]. A weak increase of γ with $\sigma^2 + \left(\frac{r^0_{A-site}}{<r_{A-site}>}\right)^2 (<r_{A-site}> - r^0_{A-site})^2$was observed (inset Fig. 3) presumably due to the increased degree of cation disorder. In order to evaluate whether this simple empirical equation (5) consisting of tabulated values of ionic radii, could be used for the selection of compositions with specific values of T_C, two compounds (series C) were prepared with an intended T_C of 35 °C. The Ca doping on A site, y, in $Ba_{1-x-y}Sr_xCa_yTiO_3$ was fixed at y = 0 and 0.1, respectively. A good agreement between the intended and measured values of T_C were observed (31 °C for 0 and 37 °C for 0.1 Ca doped samples).

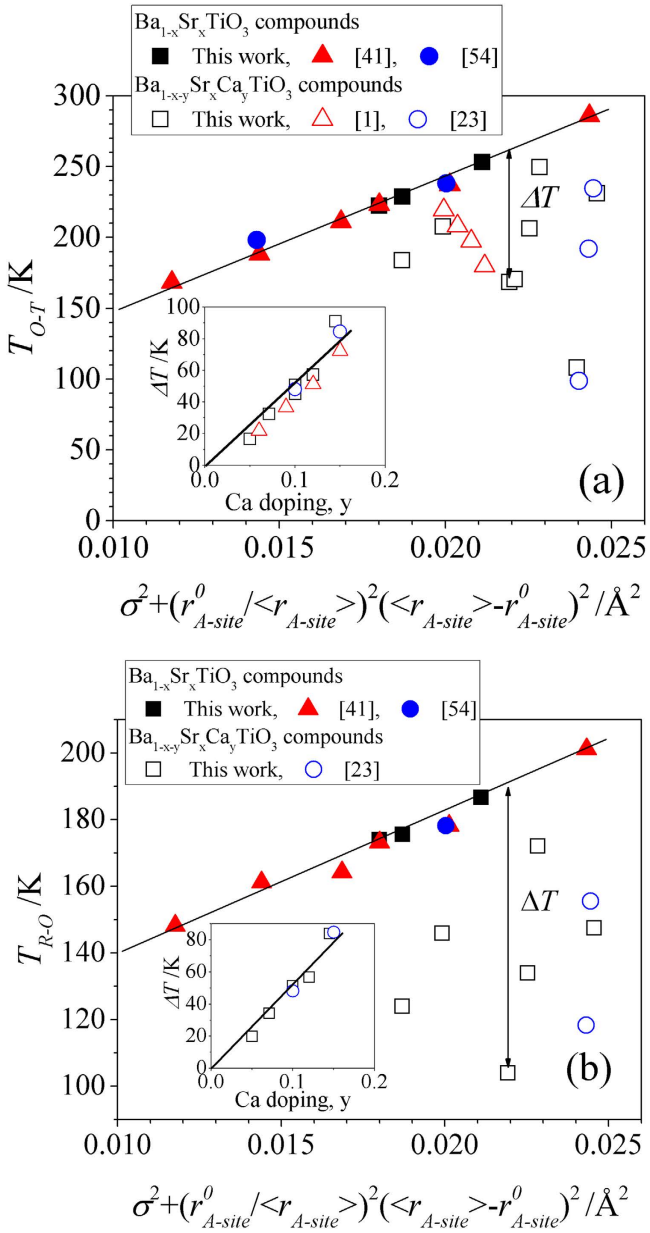

Figure 7. Temperatures of orthorhombic to tetragonal transition, $T_{O\text{-}T}$, (**a**) and rhombohedral to orthorhombic transition, $T_{R\text{-}O}$, (**b**) as function of $\sigma^2 + \left(\frac{r^0_{A-site}}{<r_{A-site}>}\right)^2 (<r_{A-site}> - r^0_{A-site})^2$. The temperature deviation, ΔT, of Ca containing samples ($Ba_{1-x-y}Sr_xCa_yTiO_3$, open symbols) from line for only Ba, Sr containing compounds ($Ba_{1-x}Sr_xTiO_3$, solid symbols). Insets show ΔT as a function of Ca doping, y. Solid lines are guides to eye.

Neutron diffraction data were collected at room temperature on several samples using the high resolution powder diffractometer, HRPD, at the ISIS neutron facility, Rutherford Appleton Laboratories, UK. Diffraction patterns were recorded over the time-of-flight range 31–125 ms, corresponding to a *d*-spacing range 0.65–2.58 Å, or 0.85–3.89 Å, for patterns collected in the back-scattering and 90 degree detector banks, respectively. The patterns were recorded to a total incident proton beam of about 60 μA h. The neutron patterns from back scattered and 90 degree banks were fitted simultaneously by Rietveld profile refinement method using Gsas II software[39]. The data were refined in P4 mm space group with the following atomic positions: Ti (0, 0, 0), Ba/Sr/Ca (0.5, 0.5, z), O1 (0, 0, z), O2 (0, 0.5, z). Due to strong correlation, atomic positions and isotropic thermal factors for A-site cations were not refined independently. As a result we were unable to model Ca ion off-centering ions as discussed above. The cation occupancies were fixed according to the results of the chemical analysis and the full oxygen occupancy was assumed. The following parameters were refined: background coefficients, scale factors, diffractometer constant, peak shape, anisotropic strain, atomic positions and isotropic displacement parameters. The results of the refinements are given in the Table 3. As a function $\sigma^2 + \left(\frac{r^0_{A-site}}{<r_{A-site}>}\right)^2 (<r_{A-site}> - r^0_{A-site})^2$ increased,

one Ti-O1 bond monotonically increased whereas another Ti-O1 bond decreased leading to the distortion of TiO_6 octahedra (Fig. 4). As a result a linear increase of the squared atomic displacement of Ti ions from the centrosymemtric position, d^2, is observed (inset Fig. 4).

Figure 5 shows the T_C as a function of $\sigma^2 + \left(\frac{r^0_{A-site}}{<r_{A-site}>}\right)^2 (<r_{A-site}> - r^0_{A-site})^2$ in a large number of $Ba_{1-x-y}Sr_xCa_yTiO_3$ with the tolerance factor greater than 1 reported in the literature over the last 60 years[12,20,40–59]. A strong linear correlation is observed with some scatter of data presumably due to compositional inhomogeneity (including partial substitution of Ca on B site[52]), annealing conditions[5], thermal hysteresis during the measurements[43], etc. In datasets[44,46] that showed a deviation from the observed empirical trend, frequency dependences of ε_r was observed in heavily doped Ca samples. As a result we suggest that the observed empirical equation (5) is valid for typical ferroelectrics.

It is interesting to consider the effect of Ca doping on T_C in $Ba_{1-y}Ca_yTiO_3$ compounds. It has been shown that Ca doping on A-site results in first slight increase of T_C with up to 8% Ca doping followed by a decrease[20,30,44,51], whereas even small extend of Ca doping on B site resulted in a drastic decrease of T_C[51,57,58] (Fig. 6). From the proposed model the introduction of smaller Ca ions in $BaTiO_3$ resulted in the increase of σ^2 and the decrease of $<r_{A-site}> - r^0_{A-site}$ thus exhibiting opposite effects on the values of T_C. As a result Tc is expected to show the maximum with Ca doping. When the T_C data was replotted as a function of $\sigma^2 + \left(\frac{r^0_{A-site}}{<r_{A-site}>}\right)^2 (<r_{A-site}> - r^0_{A-site})^2$ a monotonic increase of T_C was observed (inset to Fig. 6) regardless of Ca doping on A- or B-sites (r^0_{A-site} increased with Ca doping on the Ti-site). Furthermore our preliminary results showed that the correlation similar to (5) exists in Zr and Sn doped titanates. As a result it is possible that the observed empirical correlation (5) is valid for the families of titanates with A- and B-sites doped by isoelectronic ions. At the same time the proposed model is expected to break down when the ion shape cannot be considered spherical, for example when the stereochemically active electron lone pairs (Pb^{2+}, Bi^{3+}) or partially filled orbitals (La^{3+}) are present as shown in Supplementary Fig. S7.

The temperatures for rhombohedral to orthorhombic, $T_{R\text{-}O}$, and orthorhombic to tetragonal, $T_{O\text{-}T}$, transitions in BSCT are shown in Fig. 7(a,b), respectively. For compounds containing only Ba and Sr on the A-site, a linear increase of the transition temperatures with $\sigma^2 + \left(\frac{r^0_{A-site}}{<r_{A-site}>}\right)^2 (<r_{A-site}> - r^0_{A-site})^2$ was observed. The Ca containing samples showed negative deviation of $T_{R\text{-}O}$ and $T_{O\text{-}T}$ from the linear trends of $Ba_{1-x}Sr_xTiO_3$ compounds (marked as ΔT on Fig. 7(a,b)). ΔT increased linearly with Ca doping, y, regardless of Sr and Ba content (insets to Fig. 7 (a,b)). The following empirical equations were proposed:

for orthorhombic to tetragonal transition ($y < 0.2$)

$$T_{O-T}[K] = 9010 \times \left[\sigma^2 + \left(\frac{r^0_{A-site}}{<r_{A-site}>}\right)^2 (<r_{A-site}> - r^0_{A-site})^2\right] - 521 \times y - 61.4 \quad (6)$$

for rhombohedral to orthorhombic transition ($y < 0.15$)

$$T_{R-O}[K] = 4046 \times \left[\sigma^2 + \left(\frac{r^0_{A-site}}{<r_{A-site}>}\right)^2 (<r_{A-site}> - r^0_{A-site})^2\right] - 519 \times y - 100.0 \quad (7)$$

In conclusion we demonstrated a combined effect of average ionic radii and cation variance on T_C a $Ba_{1-x-y}Sr_xCa_yTiO_3$ ferroelctric perovskites. T_C increased linearly with σ^2 and $<r_{A-site}>$. A set of empirical equations was proposed which allowed the estimation of temperature of phase transitions in alkaline-earth titanates based on the tabulated values of ionic radii. This provides simple guidelines for a selection of compounds with required values phase transitions temperatures (T_C, $T_{R\text{-}O}$ and $T_{O\text{-}T}$) in $Ba_{1-x-y}Sr_xCa_yTiO_3$ perovskites.

References

1. Wang, J., Zhang, X., Zhang, J., Li, H. & Li, Z. Dielectric and piezoelectric properties of $(1-x)Ba_{0.7}Sr_{0.3}TiO_3-xBa_{0.7}Ca_{0.3}TiO_3$ perovskites. *J. Phys. Chem. Solids* **73,** 957–960 (2012).
2. Lin, G. C., Xiong, X. M., X., Z. J. & Wei, Q. Latent heat study of phase transition in $Ba_{0.73}Sr_{0.27}TiO_3$ induced by electric field. *J. Therm. Anal. Calorim.* **81,** 41–44 (2005).
3. Rödel, J. *et al.* Perspective on the Development of Lead-free Piezoceramics. *J. Amer. Ceram. Soc.* **92,** 1153–1177 (2009).
4. Hennings, D., Schnell, A. & Simon, G. Diffuse ferroelectric phase transitions in $Ba(Ti_{1-y}Zr_y)O_3$ ceramics. *J. Amer. Ceram. Soc.* **65,** 539–544 (1982).
5. Lee, S., Rossetti, G. A., Liu, Z.-K. & Randall, C. A. Intrinsic ferroelectric properties of the nonstoichiometric perovskite oxide $Ba_{1-x}Ti_{1-y}O_{3-x-2y}$. *J. Appl. Phys.* **105,** 093519 (2009).
6. Zhang, L., Zhong, W. L., Wang, Y. G. & Zhang, P. L. The cell volume effect in barium strontium titanate. *Solid State Commun.* **104,** 263–266 (1997).
7. Eitel, R. E. *et al.* New high temperature morphotropic phase boundary piezoelectrics based on $Bi(Me)O_3$–$PbTiO_3$ ceramics. *Jap. J. Appl. Phys.* **40,** 5999 (2001).
8. Nakamura, T., Shan, Y. J., Sun, P.-H., Inaguma, Y. & Itoh, M. Discrimination of ferroelectrics from quantum paraelectrics among perovskite titanates $ATiO_3$ and $(A'_{1/2}\,A''_{1/2})TiO_3$. *Ferroelectrics* **219,** 71–81 (1998).
9. Hidaka, T. Isotope effect on the ferroelectric phase transitions in $BaTiO_3$, $SrTiO_3$ and $PbTiO_3$. *Ferroelectrics* **283,** 11–22 (2003).
10. Zhong, W. L. *et al.* Phase transition in $PbTiO_3$ ultrafine particles of different sizes. *J. Phys. Cond. Matt.* **5,** 2619 (1993).
11. Li, W., Xu, Z., Chu, R., Fu, P. & Hao, J. Sol-gel synthesis and characterization of $Ba_{1-x}Sr_xTiO_3$ ceramics. *J. Alloys Compound.* **499,** 255–258 (2010).
12. Samara, G. A. Pressure and temperature dependences of the dielectric properties of the perovskites $BaTiO_3$ and $SrTiO_3$. *Phys. Rev.* **151,** 378–386 (1966).

13. Haeni, J. H. *et al.* Room-temperature ferroelectricity in strained $SrTiO_3$. *Nature* **430,** 758–761 (2004).
14. Yamanaka, T., Hirai, N. & Yutaka, K. Structure change of $Ca_{1-x}Sr_xTiO_3$ perovskite with composition and pressure *Amer. Mineralogist* **87,** 1183–1189 (2002).
15. Rodriguez-Martinez, L. M. & Attfield, J. P. Cation disorder and size effects in magnetoresistive manganese oxide perovskites. *Phys. Rev. B* **54,** R15622–R15625 (1996).
16. Sinclair, D. C. & Attfield, P. J. The influence of A-cation disorder on the Curie temperature of ferroelectric $ATiO_3$ perovskites. *Chem. Comm.*, **16,** 1497–1498 (1999).
17. MacManus-Driscoll, J. L. *et al.* Systematic enhancement of in-field critical current density with rare-earth ion size variance in superconducting rare-earth barium cuprate films. *Appl. Phys. Lett.* **84,** 5329–5331 (2004).
18. Shannon, R. D. Revised effective ionic radii and systematic studies of interatomic distances in halides and chalcogenides. *Acta Cryst.* **A32,** 751–767 (1976).
19. Tiwari, V. S., Singh, N. & Pandey, D. Structure and properties of (Ba,Ca)TiO3 ceramics prepared using (Ba,Ca)TiO3 ceramics I, crystallographic and microstructural studies. *J. Amer. Ceram. Soc.* **77,** 1813–1818 (1994).
20. McQuarrie, M. & Behnke, F. W. Structural and dielectric studies in the system (Ba, Ca)(Ti, Zr)O_3. *J. Amer. Ceram. Soc.* **37,** 539–543 (1954).
21. DeVries, R. C. & Roy, R. Phase equilibria in the system $BaTiO_3$—$CaTiO_3$. *J. Amer. Ceram. Soc.* **38,** 142–146 (1955).
22. Navi, N. U. *et al.* Thermochemistry of $(Ca_xSr_{1-x})TiO_3$, $(Ba_xSr_{1-x})TiO_3$, and $(Ba_xCa_{1-x})TiO_3$ perovskite solid solutions. *J. Amer. Ceram. Soc.* **95,** 1717–1726 (2012).
23. Zhu, X. N., Zhang, W. & Chen, X. M. Enhanced dielectric and ferroelectric characteristics in Ca-modified $BaTiO_3$ ceramics. *AIP Advances* **3,** 082125 (2013).
24. Fu, D., Itoh, M., Koshihara, S.-y., Kosugi, T. & Tsuneyuki, S. Anomalous Phase Diagram of Ferroelectric (Ba,Ca)TiO_3 Single Crystals with Giant Electromechanical Response. *Phys. Rev. Lett. J1-PRL* **100,** 227601 (2008).
25. Puli, V. S. *et al.* Barium zirconate-titanate/barium calcium-titanate ceramics via sol–gel process: novel high-energy-density capacitors. *J. Phys. D: Appl. Phys.* **44,** 395403 (2011).
26. Uchino, K. & Nomura, S. Critical exponents of the dielectric constants in diffused-phase-transition crystals. *Ferroelec. Lett.* **44,** 55–61 (1982).
27. Attfield, J. P. A Simple approach to lattice effects in conducting perovskite-type oxides. *Chem. Mater.* **10,** 3239–3248 (1998).
28. Rodríguez-Martínez, L. M. & Attfield, J. P. Disorder-induced orbital ordering in $L_{0.7}M_{0.3}MnO_3$ perovskites. *Phys. Rev. B* **63,** 024424 (2000).
29. Levin, I., Krayzman, V. & Woicik, J. C. Local structure in perovskite $Ba_{1-x}Sr_xTiO_3$: Reverse Monte Carlo refinements from multiple measurement techniques. *Phys. Rev. B* **89,** 024106 (2014).
30. Levin, I., Krayzman, V. & Woicik, J. C. Local-structure origins of the sustained Curie temperature in (Ba,Ca)TiO_3 ferroelectrics. *Appl. Phys. Lett.* **102,** 162906 (2013).
31. Abrahams, S. C., Kurtz, S. K. & Jamieson, P. B. Atomic displacement relationship to Curie temperature and spontaneous polarization in displacive ferroelectrics. *Phys. Rev.* **172,** 551–553 (1968).
32. Deng, H.-Y., Lam, C. H. & Huang, H. An atomistic approach to the dielectric modes of $BaTiO_3$ and $SrTiO_3$. *Solid State Commun.* **151,** 474–477 (2011).
33. Grinberg, I. & Rappe, A. M. Local structure and macroscopic properties in $PbMg_{1/3}Nb_{2/3}O_3$-$PbTiO_3$ and $PbZn_{1/3}Nb_{2/3}O_3$-$PbTiO_3$ solid solutions. *Phys. Rev. B* **70,** 220101 (2004).
34. Krayzman, V. *et al.* Ca K-edge X-ray absorption fine structure in $BaTiO_3$-$CaTiO_3$ solid solutions. *J. Appl. Phy.* **113,** 044106 (2013).
35. Dawson, J. A., Sinclair, D. C., Harding, J. H. & Freeman, C. L. A-Site Strain and Displacement in $Ba_{1-x}Ca_xTiO_3$ and $Ba_{1-x}Sr_xTiO_3$ and the Consequences for the Curie Temperature. *Chem. Mater.* **26,** 6104–6112 (2014).
36. Okajima, T., Yasukawa, K. & Umesaki, N. Local structure of Ca dopant in BaTiO3 by Ca K-edge X-ray absorption near-edge structure and first-principles calculations. *J. Electron. Spectrosc. Relat. Phenom.* **180,** 53 (2010).
37. Bilc, D. I. & Singh, D. J. Frustration of Tilts and A-Site Driven Ferroelectricity in $KNbO_3$-$LiNbO_3$ Alloys. *Phys. Rev. Lett.* **96,** 147602 (2006).
38. Singh, D. J. & Park, C. H. Polar Behavior in a Magnetic Perovskite from A-Site Size Disorder: A Density Functional Study. *Phys. Rev. Lett.* **100,** 087601 (2008).
39. Toby, B. H. & Von Dreele, R. B. GSAS-II: the genesis of a modern open-source all purpose crystallography software package. *J. Appl. Crystal.* **46,** 544–549 (2013).
40. Bednorz, J. G. & Müller, K. A. $Sr_{1-x}Ca_xTiO_3$: An XY quantum ferroelectric with transition to randomness. *Phys. Rev. Lett.* **52,** 2289–2292 (1984).
41. Berbecaru, C. *et al.* Ceramic materials $Ba_{1-x}Sr_xTiO_3$ for electronics–Synthesis and characterization. *Thin Solid Films* **516,** 8210–8214 (2008).
42. Kang, D.-S., Han, M.-S., Lee, S.-G. & Song, S.-H. Dielectric and pyroelectric properties of barium strontium calcium titanate ceramics. *J. Eur. Ceram. Soc.* **23,** 515–518 (2003).
43. Lemanov, V. V., Smirnova, E. P., Syrnikov, P. P. & Tarakanov, E. A. Phase transitions and glasslike behavior in $Sr_{1-x}Ba_xTiO_3$. *Phys. Rev. B* **54,** 3151–3157 (1996).
44. Mitsui, T. & Westphal, W. B. Dielectric and X-ray studies of $Ca_xBa_{1-x}TiO_3$ and $Ca_xSr_{1-x}TiO_3$. *Phys. Rev.* **124,** 1354–1359 (1961).
45. Naik, R. *et al.* Temperature dependence of the Raman spectra of polycrystalline $Ba_{1-x}Si_xTiO_3$. *Phys. Rev. B* **61,** 11367–11372 (2000).
46. Sakamoto, N., Wang, R. & Itoh, M. Effects of A-site ion size mismatch on dielectric properties of $SrTiO_3$. *Ferroelectrics* **262,** 131–136 (2001).
47. Syamaprasad, U., Galgali, R. K. & Mohanty, B. C. Dielectric properties of the $Ba_{1-x}Sr_xTiO_3$ system. *Mater. Lett.* **7,** 197–200 (1988).
48. Yun, S. & Wang, X. Dielectric properties of $(Ba_{1-2x}Sr_xCa_x)TiO_3$ ferroelectric ceramics. *J. Electroceram.* **21,** 585–588 (2008).
49. Wang, R., Inaguma, Y. & Itoh, M. Dielectric properties and phase transition mechanisms in $Sr_{1-x}Ba_xTiO_3$ solid solution at low doping concentration. *Materials Research Bulletin* **36,** 1693–1701 (2001).
50. Zhang, L. *et al.* Comment on the use of calcium as a dopant in X8R $BaTiO_3$-based ceramics. *Appl. Phys. Lett.* **90,** 142914 (2007).
51. Zhang, L. L., Wang, X. S., Yang, W., Liu, H. & Yao, X. Structure and relaxor behavior of $BaTiO_3$-$CaTiO_3$-$SrTiO_3$ ternary system ceramics. *J. Appl. Phys.* **104,** 5 (2008).
52. Zheng, R. K. *et al.* Effects of Ca doping on the Curie temperature, structural, dielectric, and elastic properties of $Ba_{0.4}Sr_{0.6-x}Ca_xTiO_3$ $(0 <= x <= 0.3)$ perovskites. *J. Appl. Phys.* **98,** 084108 (2005).
53. Zhou, L., Vilarinho, P. M. & Baptista, J. L. Dependence of the structural and dielectric properties of $Ba_{1-x}Sr_xTiO_3$ ceramic solid solutions on raw material processing. *J. Eur. Ceram. Soc.* **19,** 2015–2020 (1999).
54. Alexandru, H. V., Berbecaru, C., Ioachim, A., Nedelcu, L. & Dutu, A. BST solid solutions, temperature evolution of the ferroelectric transitions. *Appl. Surf. Sci.* **253,** 354–357 (2006).
55. Fu, C., Yang, C., Chen, H., Wang, Y. & Hu, L. Microstructure and dielectric properties of $Ba_xSr_{1-x}TiO_3$ ceramics. *Mater. Sci. Eng. B* **119,** 185–188 (2005).
56. Cheng, X. & Shen, M. Enhanced spontaneous polarization in Sr and Ca co-doped $BaTiO_3$ ceramics. *Solid State Commun.* **141,** 587–590 (2007).
57. Park, J. G., Oh, T. S. & Kim, Y. H. Dielectric properties and microstructural behaviour of B-site calcium-doped barium titanate ceramics. *J. Mater. Sci.* **27,** 5713–5719 (1992).

58. Zhuang, Z. Q., Harmer, M. P., Smyth, D. M. & Newnham, R. E. The effect of octahedrally-coordinated calcium on the ferroelectric transition of $BaTiO_3$. *Mater. Res. Bull.* **22,** 1329–1335 (1987).
59. Bai, Y., Han, X. & Qiao, L. Optimized electrocaloric refrigeration capacity in lead-free (1-x)BaZr0.2Ti0.8O3-xBa 0.7Ca0.3TiO3 ceramics. *Appl. Phys. Lett.* **102,** 252904 (2013).

Acknowledgements

The authors would like to acknowledge the EPSRC (grant EP/G060940/1) and STFC for financial support. Data underlying this article can be accessed on Zenodo at http://dx.doi.org/10.5281/zenodo.53983, and used under the Creative Commons Attribution licence.

Author Contributions

A.B. prepared samples, collected and analysed X-ray diffraction, ICP, DSC and dielectric data, performed Rietveld refinements and F.L.G. performed neutron measurements. N.A. supervised the project. All authors contributed in writing of the manuscript.

Additional Information

Supplementary information accompanies this paper at http://www.nature.com/srep

Competing financial interests: The authors declare no competing financial interests.

How to cite this article: Berenov, A. *et al.* Effect of ionic radii on the Curie temperature in $Ba_{1-x-y}Sr_xCa_yTiO_3$ compounds. *Sci. Rep.* **6**, 28055; doi: 10.1038/srep28055 (2016).